Journal of the European Ceramic Society 43 (2023) 530–541

Contents lists available at ScienceDirect

Journal of the European Ceramic Society

journal homepage: www.elsevier.com/locate/jeurceramsoc

EVA-PVA binder system for polymer derived mullite made by material extrusion based additive manufacturing

Fateme Sarraf [a,b,*], Amir Hadian [a], Sergey V. Churakov [b,c], Frank Clemens [a,**]

[a] Empa-Swiss Federal Laboratories for Materials Science and Technology, Ueberlandstrasse 129, CH-8600 Dübendorf, Switzerland
[b] University of Bern, Hochschulstrasse 6, CH-3012 Bern, Switzerland
[c] Paul Scherrer Institute, Forschungsstrasse 111, CH-5232 Villigen, Switzerland

ARTICLE INFO

Keywords:
Material extrusion (MEX) additive manufacturing
Mullite
Polyvinyl alcohol
Ethylene vinyl acetate
FDM/FFF

ABSTRACT

Low processing temperature of preceramic polymers (PCPs) makes them attractive for material extrusion based additive manufacturing (MEX-AM), earlier called fused deposition modeling (FDM). Fabrication of bulk polymer derived ceramics is challenging due to gas evolution during crosslinking leading to pores and cracks in final product. Mixture of ethylene vinyl acetate (EVA) and polyvinyl alcohol (PVA) was successfully used to generate open porosity before crosslinking step. For 3D printing, a pellet extruder was used and a PVA binder content of 50 vol% was essential for succcessful solvent debinding process in water. The effect of PVA content and different EVA grades on printability and debinding behavior was studied. EVA with a lower melt flow index (MFI) showed better compatibility with PVA additive in terms of mixing and printing. EVA with higher vinyl acetate content seems to be more favorable for later thermal debinding processes because of its higher gas permeability.

1. Introduction

Polymer derived ceramics (PDCs), introduced in the early 1960s, are obtained as a result of pyrolysis of preceramic polymers (PCPs), usually in non-oxidative atmospheres [1,2]. Organosilicon precursors with a Si backbone and O, C, N, B or H atoms [3], known as Si-based preceramic polymers, have remained a hot topic since then and there have been a lot of studies on synthesis of oxide and non-oxide ceramics like mullite [4], wollastonite [5], cordierite [6], SiAlON [7,8], SiOC [9,10], SiC [11] and so on. These polymeric compounds release gas byproducts while crosslinking followed by pyrolysis at higher temperatures to obtain an amorphous ceramic residue [12]. Fabrication of PDC structures have been demonstrated by various additive manufacturing techniques such as direct ink writing (DIW) [13,14], stereolithography [15], digital light processing (DLP) [16,17], selective laser sintering [18], material extrusion based additive manufacturing (MEX-AM) [19,20], etc [21]. Although DIW is a good candidate for printing simple geometries, fabrication of more complex geometries, overhangs, bridging or achieving high resolution is still a big challenge even by tailoring the rheological properties of the ink. DLP method is limited to the fabrication of thin and small structures [16,17] and with SLS only a low relative density of 90% for SiC ceramics could be achieved after 7 times polymer infiltration and pyrolysis (PIP) post-treatment [18]. Using MEX-AM method, closed porosity appeared in sintered parts [22].

Among various SiO_2 sources investigated to produce mullite, PCPs bring some advantages. Pyrolysis under air atmosphere can form fine silica powder that is highly reactive and can enhance the sintering kinetics to form silicate phases, like mullite [23]. Although the pure phase can be achieved by sol-gel route as well, thermoplastic nature of preceramic polymers provides the opportunity to use various plastic forming methods such as injection molding [24], extrusion [25,26], fused deposition modeling (FDM) [11,22], tape casting [27], fiber electrospinning [28], etc. Preceramic polymers can be also used as a substitute for the binder component that makes the thermal debinding less critical [29]. Obtained ceramics from PCPs are incredibly resistant to oxidation and creep as they reduce or eliminate the need for sintering additives [30,31]. Despite all the advantages of PCPs, obtaining dense ceramics using these polymers is still a challenge due to their large shrinkage and release of gaseous products (leading to high mass loss). Different studies have successfully addressed the shrinkage issue and solved it using inert or active fillers in order to control the dimensional changes throughout pyrolysis [32,33]. However, intensive gas release

* Corresponding author at: Empa-Swiss Federal Laboratories for Materials Science and Technology, Ueberlandstrasse 129, CH-8600 Dübendorf, Switzerland.
** Corresponding author.
E-mail addresses: Fateme.sarraf@empa.ch (F. Sarraf), frank.clemens@empa.ch (F. Clemens).

https://doi.org/10.1016/j.jeurceramsoc.2022.10.009
Received 20 June 2022; Received in revised form 26 September 2022; Accepted 7 October 2022
Available online 10 October 2022

due to crosslinking (polycondensation reactions) of preceramic polymers is still limiting the thickness of fabricated parts [22], especially if thermoplastic ceramic processing route is used. Using thermoplastic ceramic processing, the crosslinking of the added preceramic polymer already starts below the decomposition temperature of the thermoplastic binder additives. Due to the low gas permeability of the other thermoplastic binder components, the gaseous species generated by cross-linking form spherical closed pores that cannot be removed after sintering process [2,4].

Addition of thermoplastic polymeric components to ceramic powders is essential for thermoplastic shaping to ensure flowability. However, removal of volatile components after shaping can be challenging. In general, thermal debinding is one of the main steps to obtain ceramics through thermoplastic ceramic processing. A well-established common solution is to create interconnected pore channels by solvent debinding of one of binder components. Water soluble binder additives such as PEG (Polyethylene glycol), PVA (Polyvinyl alcohol), Agar, etc., are considered as sufficient and environmentally friendly options, and using an efficient amount of in-soluble backbone binder facilitates the solvent debinding process without risk of structural collapse [34–36]. Extraction of water-soluble binder leads to formation of an interconnected porous network from the surface to the center, which creates pathways for the escape of gaseous products generated during thermal decomposition of other binder components. Thus, cracks and blisters that appear as a result of an accumulation of decomposition gases due to low gas permeability through the structure, can be avoided. PVA is a common option for industrial applications due to its high chemical resistance, water solubility, non-toxicity and biodegradability. This linear polymer is the product of partial or full hydroxylation of polymerized vinyl acetate, and it is well known that lower hydrolysis degree improves the water-solubility of the synthesized PVA [37].

In material extrusion based additive manufacturing (MEX-AM), also known as fused deposition modeling technology, PVA filaments are already commercially available as a soluble support material. In comparison to other AM processes, MEX-AM is a simple shaping technology for ceramics with low investment costs, to produce ceramic and ceramic composite components [38–40]. Hadian et al. [41] demonstrated that 12 cm tall zirconia vase structures can be printed and sintered successfully using fused filament fabrication (FFF) method. Fabrication of ceramic parts using FDM printers requires a stiff filament, which resists the gears pressure and feeds the process continuously. On the other hand, filaments need to be flexible enough for spooling and running a print [42,43].

As an alternative to thermoplastic ceramic filament, pellets or granulates can be employed for MEX-AM process [44]. A screw extruder printing head helps if the development of stiff but flexible thermoplastic ceramic filament is not successful. In some cases, the ceramic filaments are too brittle to be printed continuously. Thermoplastic ceramic pellets are already used for other shaping processes like extrusion and injection molding, so pellet extrusion printers are becoming more popular in the ceramics industry.

In this research study, we present an improved material extrusion based additive manufacturing process of PDCs based on thermoplastic shaping approach, which allows us to avoid undesired closed pores formed during the crosslinking process of the preceramic polymer. Water-soluble PVA binder component is introduced to the thermoplastic binder system to generate an interconnected pore structure at room temperature to allow for the transport of gasses generated during crosslinking of the PCP. Printability, solvent, wick and thermal debinding along with sintering were studied by combining PVA binder with three different ethylene vinyl acetate copolymers (backbone binder) to finally achieve dense mullite ceramic parts.

2. Material and methods

2.1. Materials

To produce $3Al_2O_3$-$2SiO_2$ (3:2 mullite), alumina powder (γ-Al_2O_3) (PURALOX SCFa-140 UF3, Sasol Performance Chemicals Ltd) and polysiloxane polymer (SILRES MK, Wacker Chemie AG) were used. 11 wt% of magnesium oxide (MgO, Fluka™) was added as sintering additive. The composition is described in more detail somewhere else [5]. Polyvinyl alcohol (PVA, Sigma-Aldrich) was used as a water-soluble thermoplastic binder component and three grades of ethylene vinyl acetate copolymers (EVA) (Elvax, DuPont, International SARL) with different vinyl acetate (VA) content and melt flow index (MFI) were used to tailor the rheology, printability and debinding behavior. It is known that higher VA content provides higher softness, more flexibility and lowers the melting point of EVA polymers. On the other hand, low MFI corresponding to long polymer chains correlates with higher toughness and increases the melting point. The different thermoplastic binder components used in this study are listed in Table 1.

In Table 2, the feedstock composition used in this study having a constant ceramic loading of 40 vol%, with respect to the γ-Al_2O_3, MgO and SILRES MK powders, are listed.

2.2. Processing

Initially, PVA and EVA polymers were mixed in a torque rheometer equipped with roller-rotors (Rheomix 600, HAAKE™ PolyLab™ OS, Thermo Fisher Scientific, Germany) at 190 °C for 20 min to achieve a homogeneous mixture. Dried SILRES MK, Al_2O_3 and MgO powders were added and mixed until a torque equilibrium was reached. Extruded filaments with a diameter of 1.8 mm, fabricated by capillary rheometer (Rosand RH10, NETZSCH-Gerätebau GmbH, Germany) at 160 °C were brittle due to strong bonding between hydroxyl groups in PVA. As a result, they were chopped into small pellets to be used in a pellet printer.

A screw based FDM pellet printer (Tumaker Voladora NX+) was used to print all the feedstocks. Horizontal bar structures with length, width and height of 60, 4.8 and 3.8 mm were printed, respectively. The pellets were fed into the screw extruder using a fed hopper. The screw extruder consists of a feeding, compression and melting zone. In the compression zone, the pellets start to melt and due to the compression, the air is pass through the feeding zone. At the tip of the melting zone, a nozzle is fixed. For the screw section and the nozzle, temperatures of 180 and 210 °C were used, respectively. The bed temperature, printing speed, nozzle diameter and layer height were set to 95 °C, 8 mm/s, 0.8 mm and 0.5 mm, respectively. In Fig. 1, a schematic overview of the processing steps from mixing of the raw materials, extrusion and printing followed by solvent debinding, thermal debinding and sintering is summarized.

A mullite ceramic was obtained by post-processing of the printed structure in several steps (Fig. 1). First, PVA was dissolved in deionized water (DI water at room temperature) as a solvent debinding step lasting for 3 and 6 days. Afterward, the samples were dried at room temperature

Table 1
EVA and PVA thermoplastics used as binder components for the PCP-based ceramic feedstocks.

Binder trade name	Melting point (°C)	Vinyl acetate (%)	Melt flow index (g/10 min)*	Abbreviation for feedstock label	Elastic modulus (MPa)
Elvax 420	73	18	150	E420	42
Elvax 460	88	18	2.5	E460	52
Elvax 760	100	9.3	2	E760	140
PVA	–	–	–	P	–

* at 190 °C/ 2.16 kg

Table 2
Feedstocks compositions.

Feedstock	PVA content (vol%)	UF3 (wt%)	SILRES MK (wt%)	EVA content (wt %)	PVA content (wt %)
E[a]X[b]-60P	60	30.0	23.8	15.1	30.7
EX-50P	50	30.4	24.1	19.1	25.9
EX-40P	40	30.8	24.4	23.3	21.0

[a] E: indication for EVA polymer
[b] X: Different Elvax grade

under controlled humidity (10% RH) in a climate chamber (MKF 115, Binder, Germany). The dried samples were later placed in a box furnace (Pyrotec PC 12, Michel Keramikbedarf, Switzerland) for wick debinding under static air atmosphere. For this debinding step, the samples were placed in an alumina powder bed at 210 °C for 48 h (Fig. 2a). For final debinding and sintering, the samples were removed from the powder bed, cleaned and placed in a high temperature furnace (LHT 03/17 D, Nabertherm GmbH). Heating profile (Fig. 2b) for the final debinding step was optimized by using model free kinetics analysis as reported by Hadian et al. [18]. Sintering program reported by Sarraf et al. was used [5]; therefore, the debound printed parts were heated up to 1600 °C for 5 h.

2.3. Characterization

To study the rheological behavior of the feedstocks at printing temperature (210 °C), a micro compounder (HAAKE™ MiniLab 3, ThermoFisher Scientific, Germany) was used. As shown by Hadian et al., the flow path of the feedstock inside the MiniLab can be changed using a bypass valve [45]. By running the instrument in circulation mode, the rheological data can be extracted using two pressure sensors placed inside a slit geometry. Subsequently, rheological measurements were performed in a range of rotation speeds from 100 to 10 rpm in five steps. Apparent viscosity as a function of shear rate was calculated for all the different feedstock compositions.

Pore formation at low temperatures (140, 180 and 220 °C) was investigated. Higher temperatures were not investigated because wicking step was done at 210 °C. To study the effect of solvent debinding on pore formation, green and solvent debound filaments were placed in an oven (Memmert GmbH+Co KG, Germany). The cross-section of the heat-treated filaments was investigated by optical microscope (SteREO Discovery.V20, Carl Zeiss AG, Switzerland).

Thermal analysis of the pure polymers and filaments (in green, solvent debound and partially debound state) was performed by DSC/TGA instrument (STA 449 F3 Jupiter, Netzsch GmbH, Germany) with 70 ml/min air flow and heating rate of 5 K/min. In order to optimize the thermal debinding program, kinetic data (Friedman method) was analyzed by the Netzsch kinetics Neo software (Netzsch, Germany) using TG measurements with four different heating rates (2, 5, 10, and 20 k/min) up to 700 °C. Using kinetic analysis, a debinding program with a constant mass-loss rate was designed.

In addition, the cross-section of printed bars was investigated by optical microscope after each post-processing step to identify macro failures. Scanning electron microscope (SEM, VEGA 3, TESCAN, Czech Republic) was employed to study the microstructure of polished cross-section after sintering.

X-ray diffraction analysis (XRD, X'Pert PRO MPD, Malvern Panalytical Ltd, Germany) was carried out between 10 and 80 degrees at room temperature with a copper anode to evaluate the phase assemblage after sintering of the bars. The XRD patterns were analyzed using the software (HighScore, Version 4.8, Malvern Panalytical Ltd, Germany).

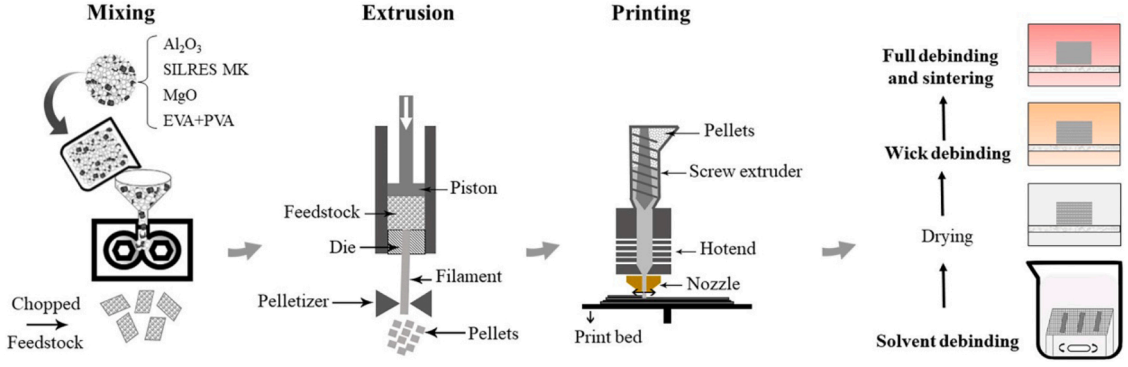

Fig. 1. Schematic overview of the processing steps from mixing until sintering for the fabrication of mullite ceramic using preceramic polymers.

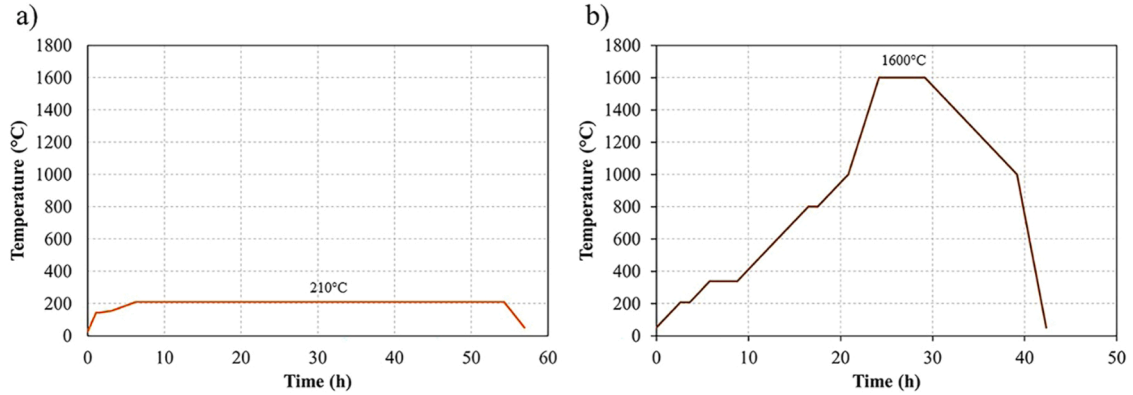

Fig. 2. Heating profile of (a) wick debinding, (b) thermal debinding and sintering used after solvent debinding of specimens.

3. Results and discussion

3.1. Flow behavior characterization of the PCP-based feedstocks

In comparison to the material properties reported by Gorjan et al. [19], the filaments produced in our study by the capillary rheometer were too brittle. This can be explained by the low thermoplasticity of PVA at its melting temperature due to strong hydrogen bonding forces between the hydroxyl groups [46]. Therefore, instead of filament based extruder head, a pellet extruder was used in this study (Fig. 1). During the extrusion step for filament fabrication with a capillary rheometer, the pressure was recorded and the results for the different feedstock recipes are shown in Fig. 3. For the Elvax 420, pressure deviation and roughness on the surface of the filaments could be observed (Fig. 3a). During the filament extrusion, extensional stress (e.g. extensional viscosity) appears at the entry of the die and this stress can cause melt rupture. This phenomenon results in pressure fluctuations and a rough surface of the extrudates. In Fig. 3b, the feedstocks with Elvax 460 are presented and both pressure curves and filament surfaces are smoother. Elvax 420 and Elvax 460 have the same vinyl acetate content but the melt flow index of the Elvax 460 is lower which can be explained by longer chain length of the polymer. The higher the molecular weight, the higher the degree of entanglement between the chains. Shorter chains have more end groups and the increase in the so-called free volume and molecular mobility of chains will result in lower Young's modulus and strength. This can result in flow instabilities and melt rupture as shown in Fig. 3a. To prove this, Elvax 760 with low MFI and low vinyl acetate content was investigated (Fig. 3c). As expected, the feedstocks made with Elvax 760 result in smoother pressure curves and filament surfaces.

Generally, the extrusion pressure increases with increasing the PVA content. The extrusion pressure for the feedstocks based on EVA with higher MFI (Elvax 420) is significantly lower. In Fig. 3a, it can be seen that the pressure increases with increasing the PVA content. As mentioned by Ku et al., PVA has a low thermoplasticity [46]. Decreasing the thermoplasticity of the feedstock will increase the extrusion pressure, which is observed for all three different EVA polymeric binders.

To avoid flow instabilities during rheological characterization of the feedstocks based on EVA 420, it was decided to use the MiniLab 3 equipment. As observed in the extrusion experiments (Fig. 3), a higher apparent viscosity was obtained by increasing the PVA content (Fig. 4), because of the lower thermoplasticity of PVA in comparison to EVA. Due to the high viscosity of E460–60P feedstock, the material was pushed out from the MiniLab (Fig. 4b); therefore, the rheological results are not reported. Typically, thermoplastic materials show shear-thinning behavior due to the entanglement of the polymer chains under shear stress. The shear-thinning behavior can be quantitatively analyzed by using the Power law equation, e.g. Ostwald–de Waele relationship (1):

$\sigma = \eta\gamma^n$ (1) σ: shear stress, η: apparent viscosity, γ: shear rate, n: power law index.

A power law index below 1 indicates shear-thinning behavior. The lower the power law index, the higher the shear-thinning effect. As shown in Fig. 4d, an increase in PVA content results in a higher shear sensitivity and greater pseudoplastic behavior of the feedstocks.

Heiber et al. reported that higher powder content in ceramic feedstocks results in lower power law index [47]. They explained that higher shear thinning effect occurs because the effective gap length in which the polymer can be sheared decreases. A lower gap length will result in higher internal shear stress and leads to a decrease in the viscosity and consequently, to a convergence of the viscosity values at higher powder loading contents. It can be assumed that a similar effect will occur when mixing a polymer with low thermoplasticity, e.g. PVA, with EVA (high thermoplasticity).

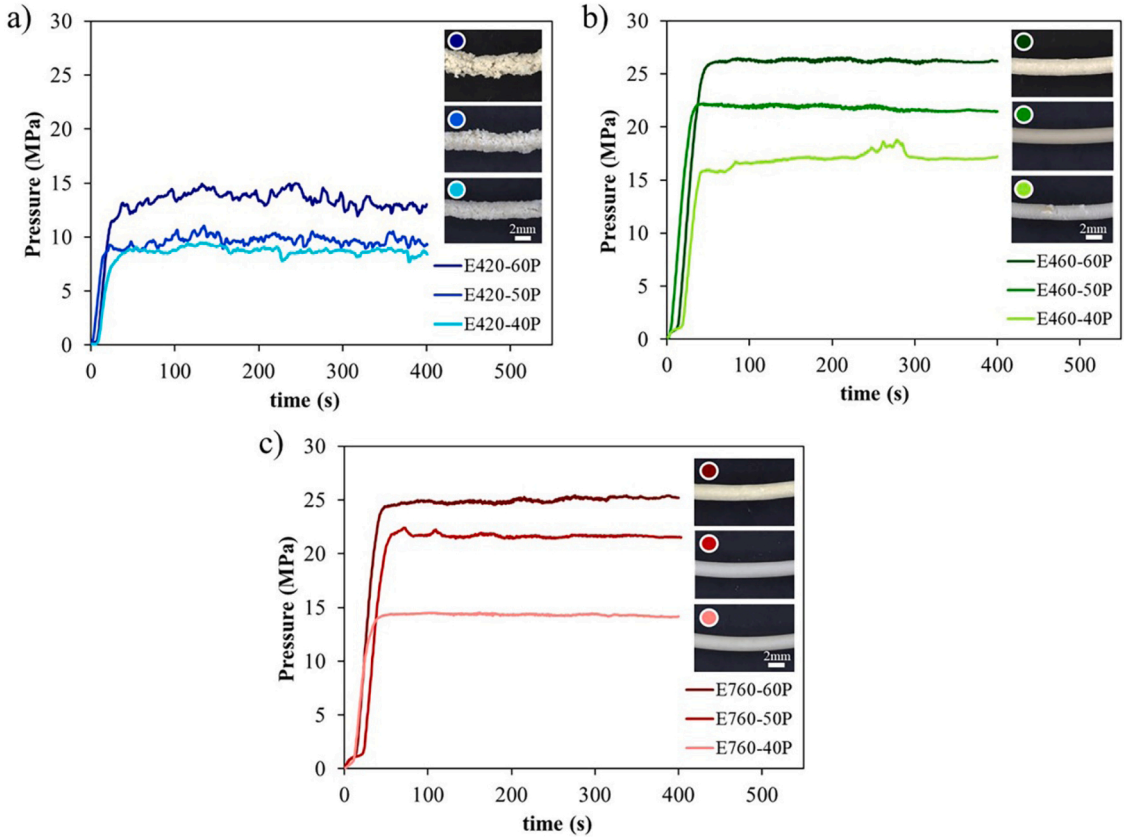

Fig. 3. Pressure versus time plots of extruded filaments with (a) E420, (b) E460 and (c) E760 containing 40, 50 and 60 vol% PVA. For the extrusion of the filaments, a temperature of 160 °C and a die orifice of 1.8 mm was used.

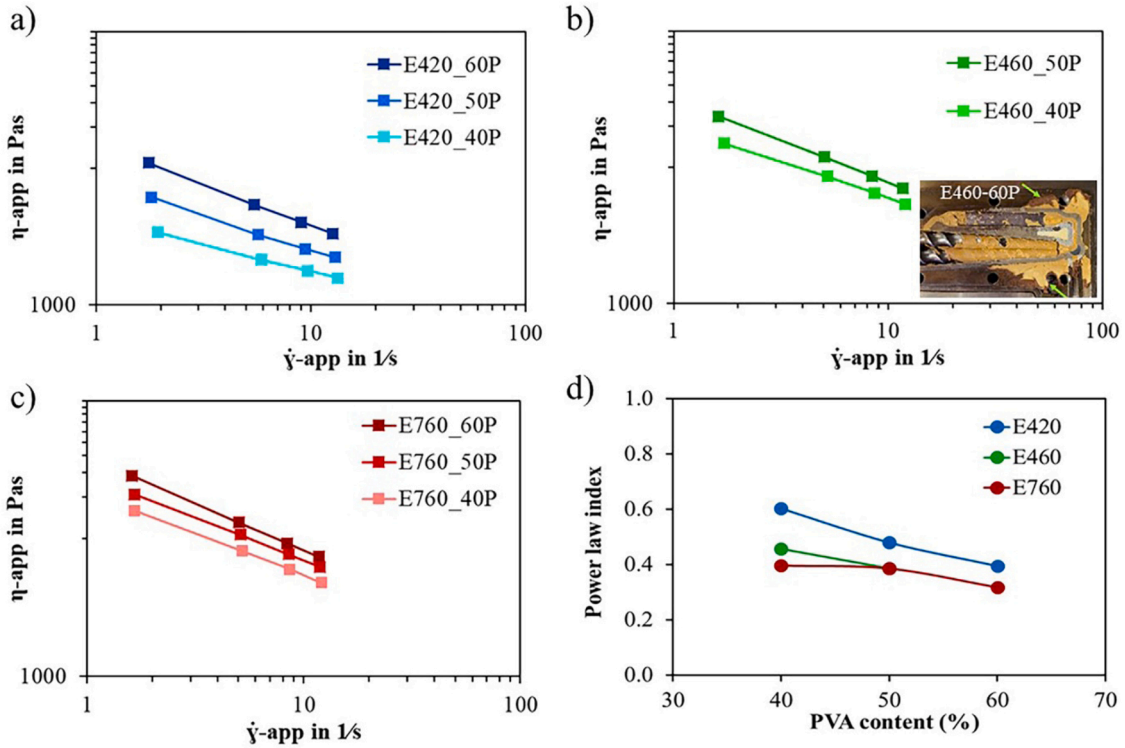

Fig. 4. Apparent viscosity versus shear rate plots for (a) E420, (b) E460 and (c) E760 with 40, 50 and 60 vol% PVA. (d) Power law index calculated for all nine compositions. The analyses were performed at 210 °C.

3.2. Investigation of pore formation during crosslinking of the PCP-based feedstocks

To investigate the efficiency of the solvent debinding in order to avoid pore formation during crosslinking of preceramic polymers, E760–50P green and solvent debound filaments were heat treated at 140, 180 and 220 °C for one hour. Fig. 5a shows that there is no evidence of pore formation up to 180 °C and by increasing the temperature to 220 °C, the pores start to appear, due to the gas evolution during the crosslinking of SILRES MK. However, by solvent debinding of the PVA binder additive, the pore formation can be avoided (Fig. 5b). Therefore, the obtained interconnected porous network after the PVA removal is sufficient to ensure the gas release during the crosslinking (polycondensation reactions) of the PCP.

3.3. Development of debinding program by kinetics analysis

Since the solvent debinding concept was successful in gas removal during crosslinking of the preceramic polymer (PCP), we further investigated the debinding process by model-free kinetics analysis. Solvent debound filaments of E760–50P were used to optimize further debinding steps. Constant mass-loss rate of 0.04%/min was selected conservatively to optimize the debinding program for the solvent debound and wick debound ceramic parts.

Investigation of the debinding behavior for solvent debound PCP based ceramic filaments.

Kinetic modeling of the solvent debound filaments presented in Fig. 6a, shows a drop in activation energy between 0.55 and 0.7 conversion values. This can be interpreted as an exothermic reaction [18]. This exothermic reaction is responsible for an overheating in the sample

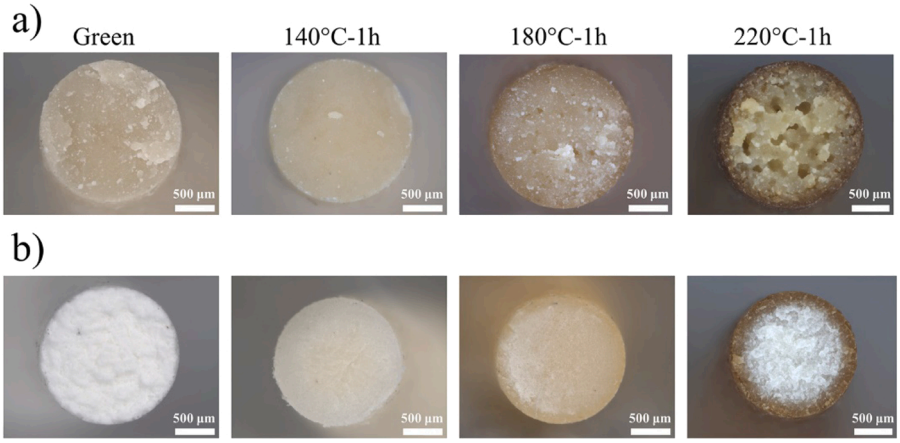

Fig. 5. Optical microscope analysis of Elvax 760–50P filament cross-sections after heat treatment at 140, 180 and 220 °C for (a) green filament, (b) solvent debound filament (DI water for 6 days at 25 °C).

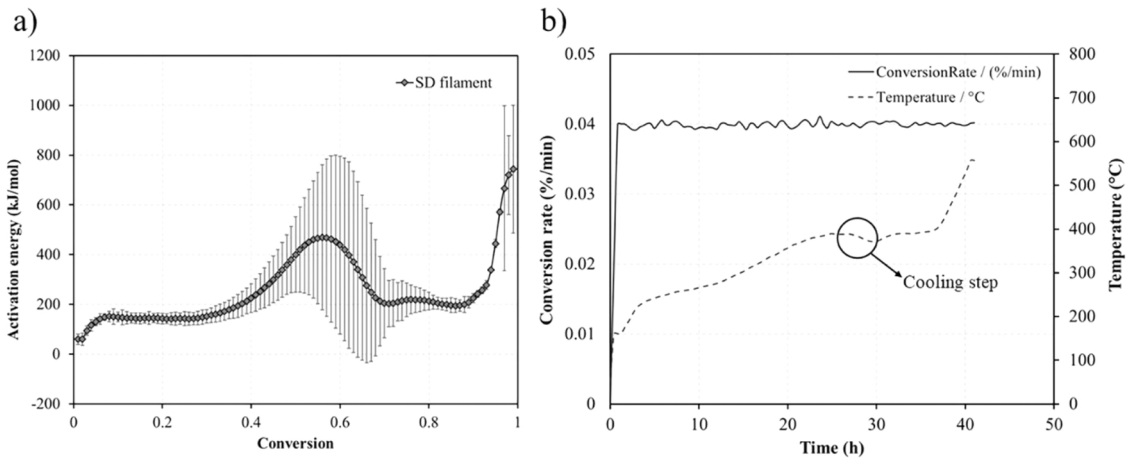

Fig. 6. (a) Kinetic modeling of the thermal debinding process for solvent debound E760–50P filament and (b) debinding program with a constant mass-loss rate of 0.04%/min.

and subsequently higher mass loss rate can be expected. This phenomenon can result in formation of blisters and crack in the sample. To avoid these issues, a cooling step is needed at around 390 °C for 5 h (Fig. 6b). Accordingly, a multistep debinding approach was employed. First, a wick debinding step at 210 °C was added. This is the temperature in Fig. 6b, at which the heating rate is decreasing due to higher binder mass loss.

The wicking step represents an isothermal heat treatment for several hours aimed to remove binder of the printed and solvent debound parts retained by capillary forces. To set up the wicking program, solvent debound E760–50P filaments were heat treated at 210 °C for 4, 8 and 48 h. It can be seen in Fig. 7 that 4 and 8 h dwell time at 210 °C are not sufficient to remove the binder from the whole volume of filaments. It is obvious that during wicking debinding, mass is transported out of the sample through already gained pores by mainly capillary forces and pressure driven liquid transport; therefore, it can be expected that the

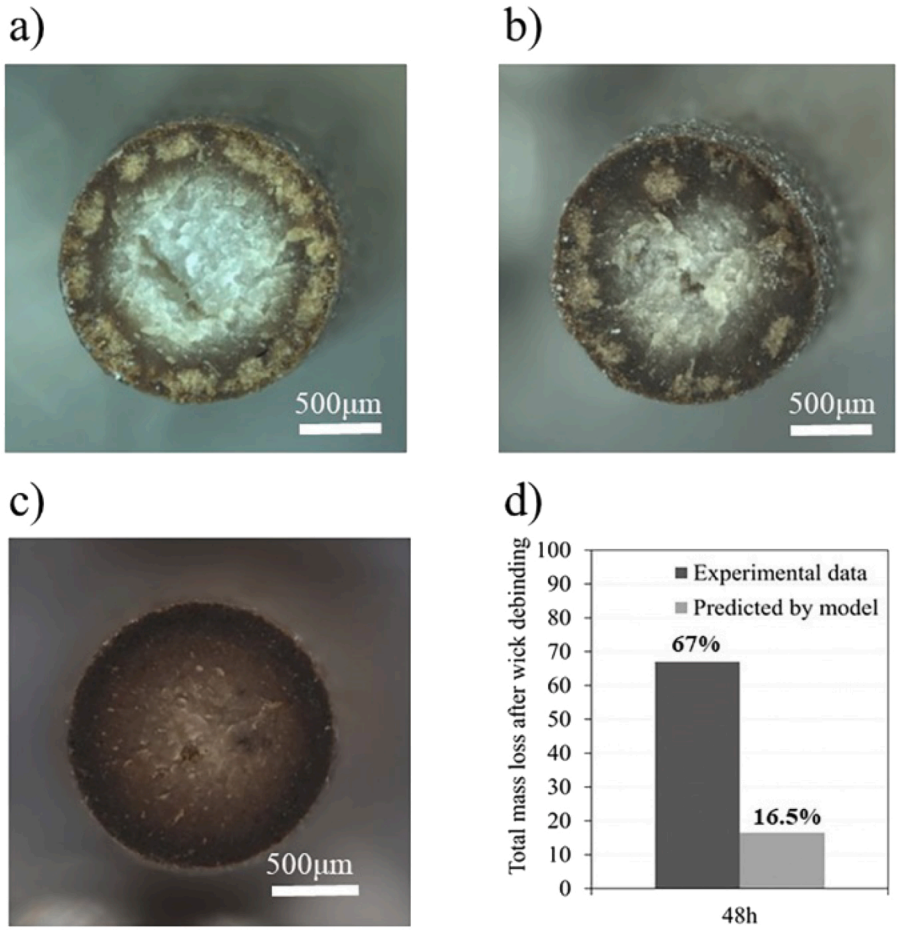

Fig. 7. Cross-section of E760–50P filaments after wick debinding at 210 °C for (a) 4, (b) 8 and (c) 48 h. Total mass loss weighed by balance (experimental data) and predicted using free-model kinetic simulated data after 48 h dwell time.

wicking process for the printed bars will be longer in comparison to the filaments. Due to this reason, we decided to significantly increase the wicking time up to 48 h (Fig. 7c). In Fig. 7d, the mass loss after wicking for 48 h is shown. It can be seen that the mass loss calculated by free-model kinetics and experimentally analyzed data differ by a factor of 4. As a result, we can conclude that isothermal debinding process cannot be modeled by free-model kinetics due to additional parameters like capillary forces, which have remarkable effect on the debinding process.

After wick debinding, thermal debinding program was investigated again by model-free kinetics. As presented in Fig. 8a, activation energy is flattened and a full debinding program without a cooling step can be achieved with a constant conversion rate of 0.04% per min.

Investigation of the thermal evolution of PCP based ceramic filaments.

In order to better understand the debinding steps in this system, thermogravimetric analysis (TG) was performed for the pure polymeric components and filaments after the printing, solvent debinding and wick debinding (Fig. 9). Decomposition and removal of volatile components can be divided into 3 different temperature zones. As can be seen in Fig. 9a, first mass loss in MK, starts in zone 1 due to polycondensation reactions during cross-linking of MK releasing water, ethanol and methanol [19]. This is followed by a second mass loss in zone 2 resulting from the polymer to ceramic conversion by removal of the organic fractions of MK. PVA also indicates an intense mass loss in zone 1 that relates to inclusion of oxygen and reduction of OH species in the polymer chains (water elimination) [48]. Second mass loss starts at around 400 °C corresponding to a 2-step rapid oxidation indicated as zone 2. It is worthwhile to mention that PVA has an amorphous carbon residue of around 1.62% (pyrolisation product) in air atmosphere at temperatures below 600 °C that will be oxidized and removed at 1000 °C (see Fig. 9a). In the case of EVA, first mass loss happens due to deacetylation of EVA polymer and loss of acetic acid [49]. The second mass loss starts around 400 °C (see zone 2) as EVA polymer continues the random chain scissoring of the remained polymer to form unsaturated vapors such as butene and ethylene and the cross-linked polyethylene structure breaks down into volatiles. Considering the TG and DTG curve of green filament, first mass loss that starts at 210 °C, results from the overlap between cross-linking of Silres MK and water elimination in PVA indicated in zone 1. At temperatures between 300 and 380 °C, a second drop appears in the green filament DTG curve as a result of the deacetylation of EVA. By increasing the temperature (zone 2), an overlap of different reactions including pyrolysis of MK, oxidation of PVA and scissoring in remaining chains from EVA can be observed. Last trough in DTG curve (zone 3) is related to loss of remained molecules from EVA between 450 and 550 °C. This forms a graphite like structure. The mentioned temperature range has shifted to higher temperatures as the diffusion of gases in the feedstock can be more difficult compared to pure polymer. According to the SD and WD-4 h DTG curves, the mentioned trough for green filament in zone 1 is no longer visible due to extracting majority of

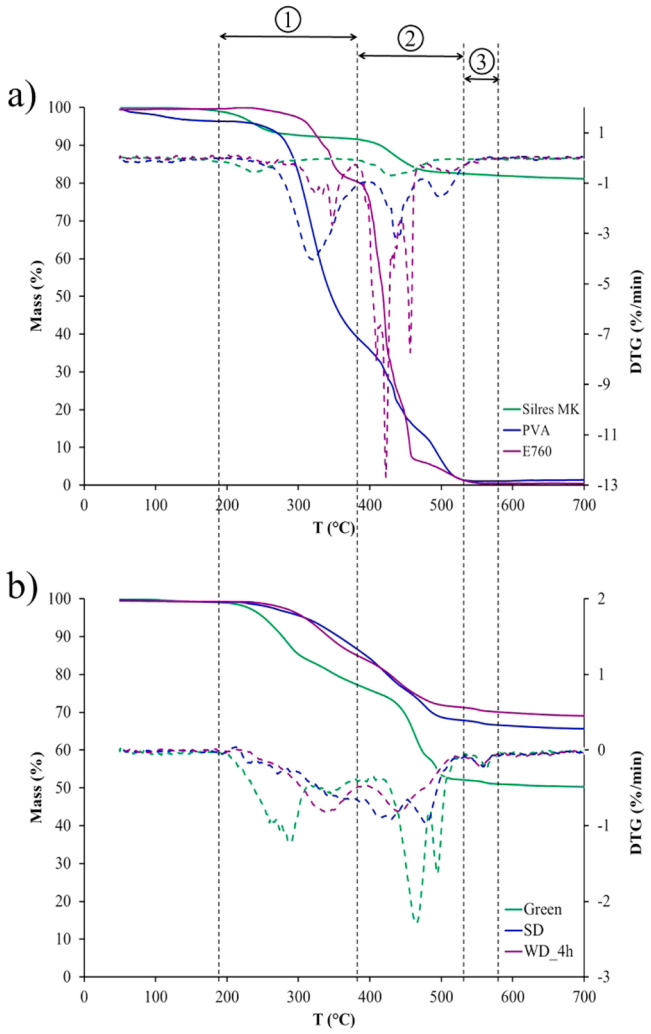

Fig. 9. (a) TG analysis of a) Silres MK, PVA and E760, b) filaments in green (G), solvent debound (SD) and wick debound (WD) indicated as TG (··) and DTG (··) versus T (°C).

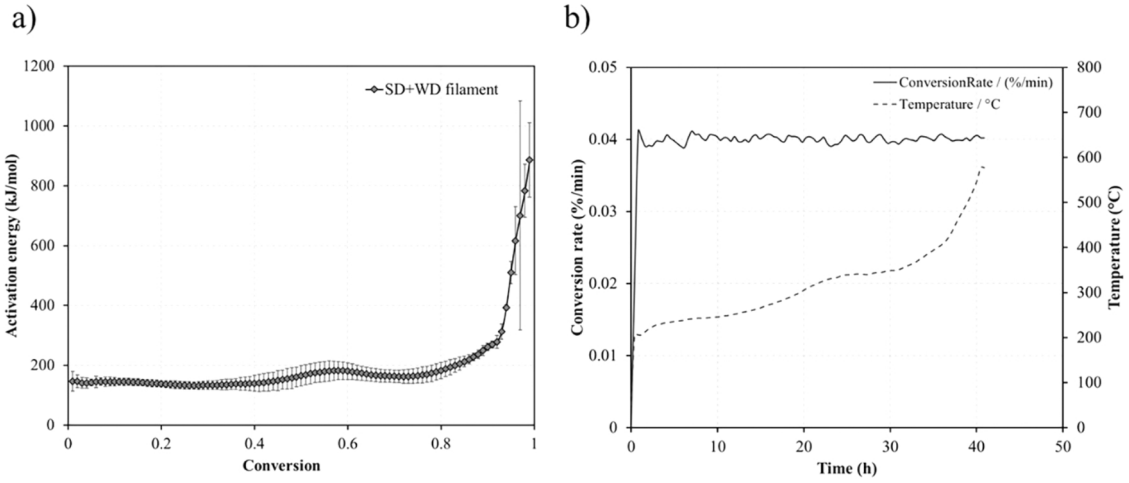

Fig. 8. (a) Kinetic modeling of the debinding process for solvent and wick debound filament E760–50P and (b) debinding program with a constant mass-loss rate of 0.04%/min.

PVA during the solvent debinding process. By increasing the temperature for SD filament (zone 2), the amount of mass loss is reduced due to dissolving the PVA in an earlier stage. The amount of mass loss for WD-4 h filament is reduced even further. This can be explained by chain scissoring and removal of some EVA molecules during the WD-4 h stage (dwell time of 4 h). Moreover, the mentioned troughs are shifted to lower temperatures as the removal of PVA (creation of porous network) facilitated the release of decomposition gases.

3.4. Printing of the PCP-based feedstocks

As can be seen in Figs. 10a, 7-layer bar structures were printed in horizontal direction. Because of the flow instabilities, the feedstocks based on Elvax 420 were not further investigated. All feedstocks with 60 vol% PVA caused clogging in the printing nozzle and the fusion between the printed layers was not sufficient (Fig. 10c). We anticipate that the high amount of PVA weakens the adhesion between the layers, due to the lower thermoplasticity. Therefore those feedstocks were not further investigated.

For the printing experiments, we focused on Elvax 460 and 760 binder compositions with 40 and 50 vol% PVA. All those feedstocks could be printed successfully with a sufficient fusion between the printed layers (Fig. 10b).

3.5. Debinding and sintering of printed PCP-based feedstocks

Green printed structures went through a debinding and sintering process. Debinding of the printed structures was performed in three steps: 1) Solvent debinding to remove the PVA and generate an interconnected porous network, 2) Wick debinding in an alumina powder bed to extend the open porosity, and 3) Full thermal debinding without a powder bed to remove the organic binder completely and sinter the ceramic at 1600 °C for 5 h.

3.5.1. Solvent debinding of printed PCP-based feedstocks

As can be seen in Fig. 11, green printed bars based on Elvax E460 with 40 and 50 vol% PVA were solvent debound in DI water for 3 and 6 days. By optical microscopy, a homogenous PVA removal after 3 days could be observed for E460–40P sample and 83% of the PVA could be removed (Fig. 11b,d). After 6 days, 90% of the PVA could be removed. Immersing E460–50P samples in water for 3 days, provided a higher PVA removal of 88% that increased to 92% after 6 days.

Interestingly, as shown in Fig. 12, the samples based on E760–40P resulted in significantly lower PVA removal after 3 days (20%) and 6 days (42%). It could be observed that the PVA removal occurs from the edges to the center of the printed bars and a core-shell structure in the samples can be identified. The dissolving mechanism of water soluble binders (e.g. PEG and PVA) can be described in three general steps [50, 51]. In the initial stage (I), sample is immersed in water. Water diffuses in PVA cause swelling and gelation on the sample surface. Water further diffuses through the swelled gel and PVA starts to dissolve from the surface into bulk, generating fine pores. At the next Intermediate stage (II), water further penetrates inside the sample and more PVA is dissolved. III) Finally, pore size, pore distribution and volume continually increase while the water starts to reach the center of the sample. Eventually, a porous interconnected network is provided that ensures the transport pathway for gas to be released during the thermal debinding of backbone binder (EVA). By increasing the PVA to 50 vol% (E760–50P samples), the amount of PVA that could be removed was similar to the E460–50P samples. Therefore, 88% and 90% of PVA could be removed after 3 and 6 days, respectively.

We conclude that PVA removal above 80% is necessary to avoid core-shell microstructure and to achieve a uniform solvent debound sample. As expected, a higher PVA content improves the solvent debinding process. However, vinyl acetate content seems to affect the process, too; therefore, three days of solvent debinding seems insufficient for the E760–40P composition. Elvax460 has two-time higher vinyl acetate content compared to Elvax760. A higher vinyl acetate results in a lower elastic modulus (Table 1). Due to the higher elastic modulus for Elvax760, the printed structure is less flexible and hinders the swelling of the PVA. Therefore, PVA removal takes longer time. Initially, solvent debinding analysis for four different times (6 h and 1, 3 and 6 days) were investigated. Considering the results, we focused on 3 and 6 days to investigate the solvent debinding process for the different PVA contents (Fig. S1).

3.5.2. Wick debinding of the printed PCP-based feedstocks

Due to the core formation of the E760–40P during solvent debinding, these samples were not further investigated. All other printed bars were further processed using wick debinding. By thermal treatment EVA and the rest of PVA binder will start to decompose in air atmosphere; therefore, the total binder mass loss is plotted in Fig. 13.

The E460–40P printed bars could not be homogeneously debound by wicking process. White parts (only solvent debound) still remained inside the samples and it can be assumed that the extent of the interconnected pore structure achieved by the solvent debinding process is not sufficient. A higher PVA content is needed to achieve desired volume of open pore channels for a successful wick debinding process, as shown by the microscopic analysis of the E460–50P samples. However, looking at the E760–50P samples, a lower vinyl acetate content of the EVA will

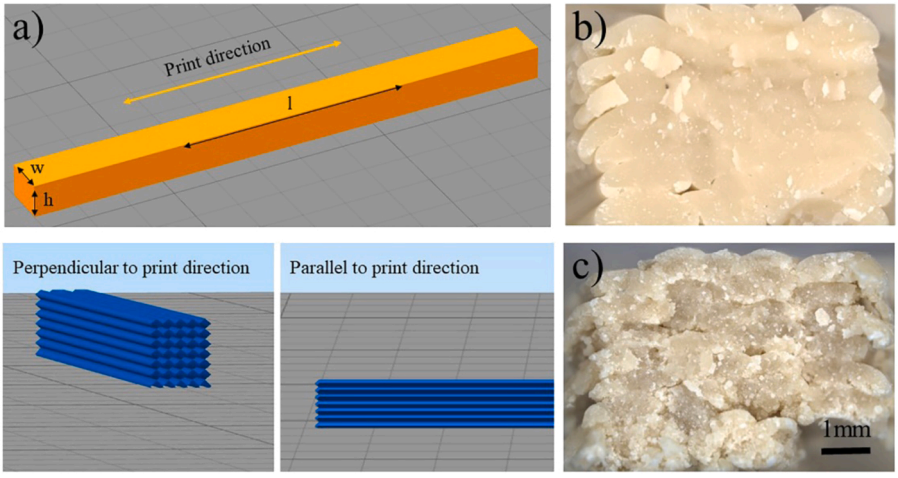

Fig. 10. (a) STL model of bar structure in Simplify3D software. (b) proper fusion between layers could be achieved with binder systems based on EVA mixed with 40 and 50 vol% PVA, (c) Introducing PVA content of 60 vol% inside the EVA binder system resulted in poor fusion between printed layers.

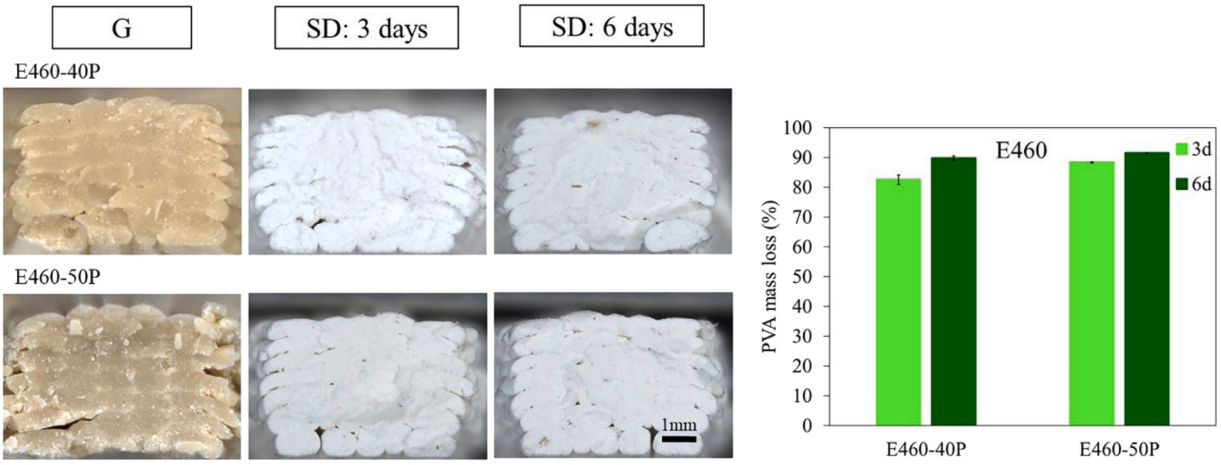

Fig. 11. Cross-section of green printed bars (G), Solvent debound bars for 3 (SD: 3 days) and 6 days (SD: 6 days) by optical microscope, from Elvax460 compositions. PVA mass loss (%) is reported for Elvax460 compositions after 3 and 6 days.

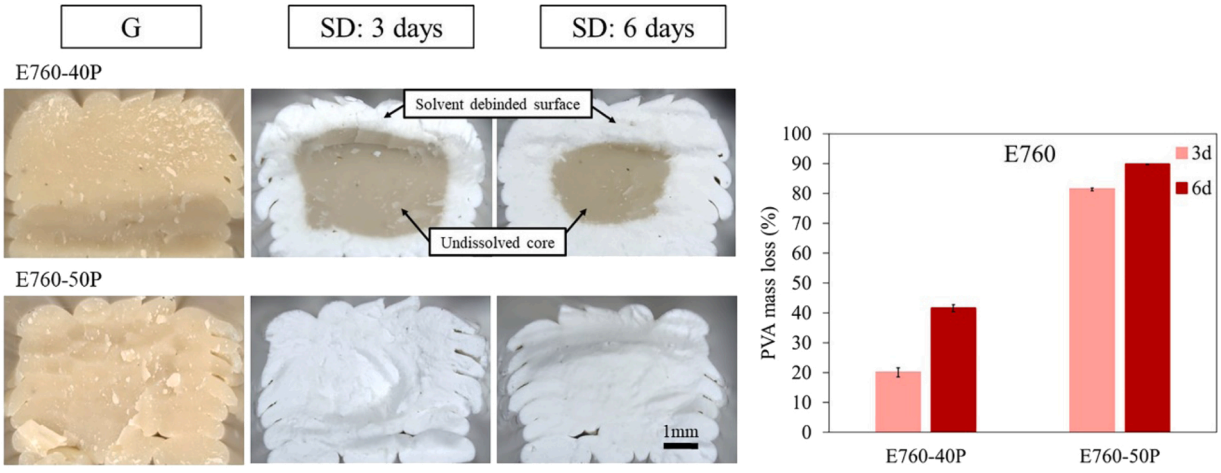

Fig. 12. Cross-section of green printed bars (G), Solvent debound bars for 3 (SD: 3 days) and 6 days (SD: 6 days) by optical microscope, from Elvax760 compositions. PVA mass loss (%) is reported for Elvax760 compositions after 3 and 6 days.

significantly reduce the wicking efficiency. This can be explained by higher gas permeability of the EVA polymers by increasing the vinyl acetate content [28]. Although wick debinding of filaments with E760–50P composition after 48 h was successful (Fig. 7), a white core remains in the printed bar with higher wall thickness. It is anticipated that the white core can be removed by increasing the wicking time. We can conclude that EVA polymer with higher vinyl acetate content should be favored to develop thermoplastic binder for ceramic processing.

The brown color, which appeared after wick debinding, indicates the thermal-oxidative degradation of thermoplastic binders leaving carbon-saturated molecules, visible by the change in color. Solvent debinding step before thermal treatment provides a porous network as a pathway for the removal of volatile components during the wicking process. As shown in Fig. 13, 50 vol% PVA content in the Elvax 460 binder system results in a sufficient wicking process. Both, Elvax 460 and 760 binders with 50 vol% PVA, showed a similarly high binder removal after 3 and 6 days of solvent debinding. However, the samples show completely different wicking behavior. As already mentioned, the main difference between the two EVAs is the vinyl acetate content. The EVA 460 has two times higher vinyl acetate content, and therefore, a higher gas permeability can be expected [28]. We can conclude that a high gas permeability of the EVA binder is helpful to achieve faster debinding at low temperatures.

It is worthwhile to mention that up to 77% of the organics can be removed after solvent and wick debinding step using the Elvax 460 binder system with 50 vol% PVA.

3.5.3. *Full debinding and sintering of the printed PCP-based Feedstocks*

Full debinding was performed up to 900 °C followed by sintering at 1600 °C for 5 h. Fig. 14 presents cross-section of sintered samples, which shows horizontal cracks and pores inside the SEM pictures of sintered parts. Those defects remain from the printing process as can be already seen in Fig. 10b. In addition to these structural defects, core-shell structure was observed in sintered parts based on E460–40P subjected to solvent debinding for 3 days. The core-shell structure is highlighted with yellow arrows and a number (1). As can be seen in Fig. 13, this sample already showed an insufficient wick debinding and a low total mass loss. It can be expected that extended solvent debinding time would allow to prevent the formation of core shell defect due to the outgassing of the decomposed organic binders. By increasing the solvent debinding time up to 6 days, 17% higher total binder mass loss could be achieved and the structural artifacts by outgassing phenomena could be avoided, as shown inFig. 13. Independent of the solvent debinding time, sintered bars made of E460–50P binder system show only residual defects related to printing process (2). The numbers of structural defects during printing are significantly higher in comparison to Elvax 460–40P binder system due to the lower thermoplasticity of the PVA. For the sintered bars based on E760–50P, after solvent debinding for 3 days, the

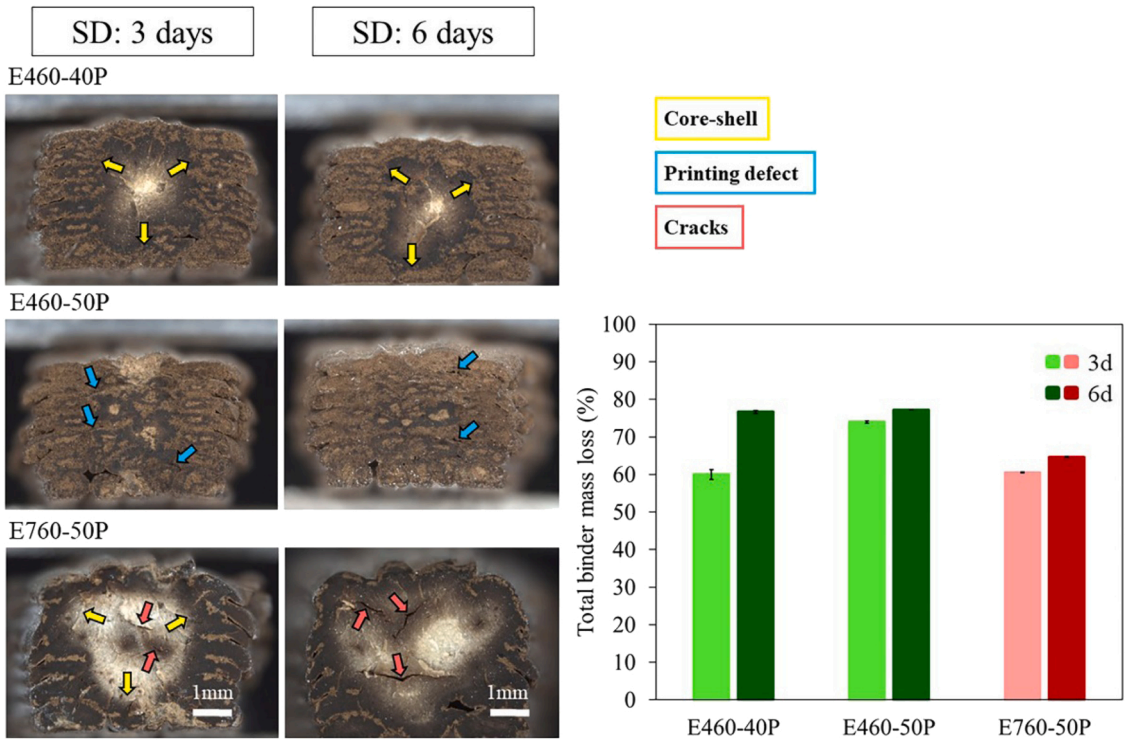

Fig. 13. Wick debinding of bars at 210 °C for 48 h, solvent debound for 3 and 6 days from different EVA-PVA binder compositions. Total binder mass loss (%) after solvent and wick debinding process is plotted for Elvax460 and Elvax760.

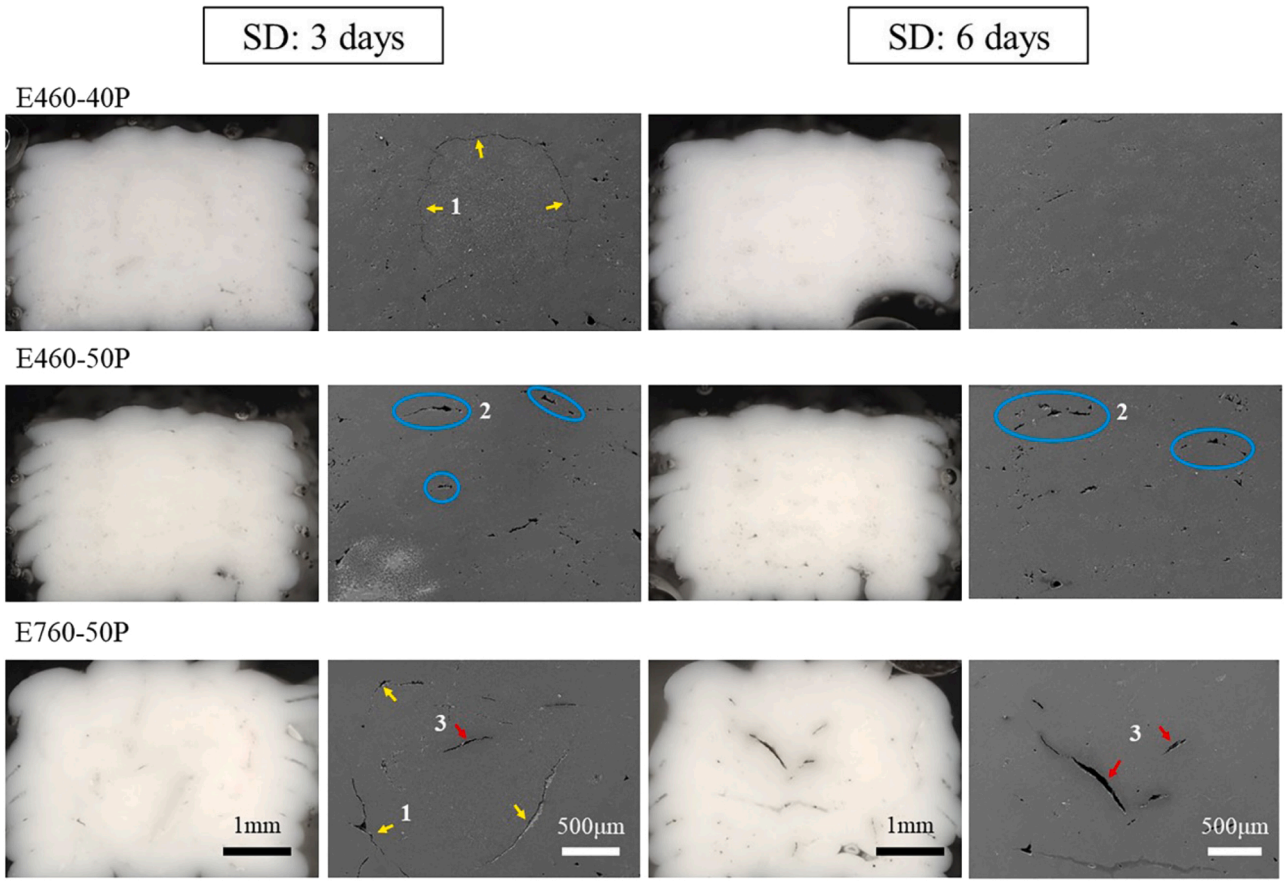

Fig. 14. Optical and scanning electron microscope images of sintered bars that were solvent debound for 3 and 6 days. Observed defects are labeled as (1) core-shell structure, (2) Printing defect and insufficient fusion between layers, and (3) crack in the center of sample.

core-shell structure (1) and cracks (3) are visible in Fig. 14. By increasing the solvent debinding time to 6 days, the core-shell structure is disappeared, however, debinding cracks (3) remained in the center of the sintered part. Elvax460 composition with 50% from each binder was considered as the optimum binder ratio as it lost a high percentage of PVA over 3 days. Nevertheless, the printing parameters may need to be optimized further. XRD analysis of E460–50P bar proved full mullitization after sintering (Fig. S2).

4. Conclusion

Polymer derived mullite ceramic structures were printed by material extrusion based additive manufacturing (MEX-AM) technique, known also as fused deposition modeling. A mixture of EVA and PVA with a ratio of 40/60, 50/50 and 60/40 vol% were studied as the binder system. Rheological behavior of feedstocks with different compositions was investigated, it could be shown that increasing PVA content increases the feedstock viscosity due to its lower thermoplasticity. Using three different EVA grades, it could be demonstrated that EVA with low molecular chain length (high MFI) results in flow instability and lead to melt rupture.

Bars with 40% and 50% PVA were successfully printed and solvent debound. A higher amount of PVA resulted in fusion problems between the layers and the orifice of the printing nozzle led to occlusion.

Removal of organic binders was performed in three steps. Initial solvent debinding in water at room temperature followed by wick debinding up to 210 °C was used. Subsequently, full thermal debinding was performed to remove all volatile components before sintering. Solvent debinding step was necessary to achieve interconnected pore channels facilitating the escape of gaseous species during cross-linking of SILRES MK and removal of decomposition gases from backbone binder during wick debinding. The amount of vinyl acetate had a positive influence on the solvent debinding of PVA. As a result, EVA with higher VA content is more suitable for ceramic processing. As the PVA starts to form a swollen gel in contact with water, EVA with a higher amount of VA should not block the swelling phenomenon of PVA and penetration of water inside the sample will be easier, because EVA with higher VA content results in lower Young's modulus. To remove the remained organics after solvent debinding, model-free kinetics studies were performed in order to design the wick and full debinding programs for the samples with a constant mass loss rate (0.04%/min). Additional wick debinding was used to avoid a cooling step during thermal debinding. Interestingly samples with E460 binder system showed a higher mass loss, which can be explained by the higher gas permeability of EVA with higher vinyl acetate content.

Finally, an investigation on the fracture surface of bar structures after sintering revealed that samples based on E460 binder system with a PVA content of 50 vol% showed the best performance. However, printing parameters have to be adjusted to avoid printing defects. It can be assumed that for the E460–50P binder system only 3 days of solvent debinding is needed to remove almost 90% of the PVA binder.

Declaration of Competing Interest

The authors declare that they have no known competing financial interests or personal relationships that could have appeared to influence the work reported in this paper.

Acknowledgements

This work was supported by the Swiss National Science Foundation (SNSF) [grant number 200021_184691/1].

Appendix A. Supporting information

Supplementary data associated with this article can be found in the online version at doi:10.1016/j.jeurceramsoc.2022.10.009.

References

[1] R. Sujith, S. Jothi, A. Zimmermann, F. Aldinger, R. Kumar, Mechanical behaviour of polymer derived ceramics–a review, Int. Mater. Rev. 66 (6) (2021) 426–449, https://doi.org/10.1080/09506608.2020.1784616.
[2] E. Bernardo, L. Fiocco, G. Parcianello, E. Storti, P. Colombo, Advanced ceramics from preceramic polymers modified at the nano-scale: a review, Materials 7 (3) (2014) 1927–1956, https://doi.org/10.3390/ma7031927.
[3] P. Colombo, G. Mera, R. Riedel, G.D. Soraru, Polymer-derived ceramics: 40 years of research and innovation in advanced ceramics, J. Am. Ceram. Soc. 93 (7) (2010) 1805–1837, https://doi.org/10.1111/j.1551-2916.2010.03876.x.
[4] E. Bernardo, P. Colombo, E. Pippel, J. Woltersdorf, Novel mullite synthesis based on alumina nanoparticles and a preceramic polymer, J. Am. Ceram. Soc. 89 (5) (2006) 1577–1583, https://doi.org/10.1111/j.1551-2916.2006.00963.x.
[5] H. Elsayed, P. Colombo, Crack-free silicate bioceramics from preceramic polymers, Adv. Appl. Ceram. 115 (4) (2016) 193–199, https://doi.org/10.1080/17436753.2015.1116663.
[6] I.H. Song, M.J. Kim, H.D. Kim, Y.W. Kim, Processing of microcellular cordierite ceramics from a preceramic polymer, Scr. Mater. 54 (8) (2006) 1521–1525, https://doi.org/10.1016/j.scriptamat.2005.12.039.
[7] G. Parcianello, E. Bernardo, P. Colombo, Z. Lenčéš, M. Vetrecín, P. Šajgalík, M. Kašiarová, Preceramic polymer-derived SiAlON as sintering aid for silicon nitride, J. Am. Ceram. Soc. 97 (11) (2014) 3407–3412, https://doi.org/10.1111/jace.13134.
[8] G. Parcianello, E. Bernardo, P. Colombo, Optimization of phase purity of β′-sialon ceramics produced from silazanes and nano-sized alumina, J. Am. Ceram. Soc. 95 (7) (2012) 148–2154, https://doi.org/10.1111/j.1551-2916.2012.05179.x.
[9] G. Pierin, C. Grotta, P. Colombo, C. Mattevi, Direct Ink Writing of micrometric SiOC ceramic structures using a preceramic polymer, J. Eur. Ceram. Soc. 36 (7) (2016) 1589–1594, https://doi.org/10.1016/j.jeurceramsoc.2016.01.047.
[10] K. Huang, H. Elsayed, G. Franchin, P. Colombo, 3D printing of polymer-derived SiOC with hierarchical and tunable porosity, Addit. Manuf. 36 (2020), 101549, https://doi.org/10.1016/j.addma.2020.101549.
[11] L. Zhao, X. Wang, H. Xiong, K. Zhou, D. Zhang, Optimized preceramic polymer for 3D structured ceramics via fused deposition modeling, J. Eur. Ceram. Soc. 41 (10) (2021) 5066–5074, https://doi.org/10.1016/j.jeurceramsoc.2021.03.061.
[12] Q. Wen, Z. Yu, R. Riedel, The fate and role of in situ formed carbon in polymer-derived ceramics, Prog. Mater. Sci. 109 (2020), 100623, https://doi.org/10.1016/j.pmatsci.2019.100623.
[13] S.S. Hossain, I.W. Baek, H.J. Son, S. Park, C.J. Bae, 3D printing of porous low-temperature in-situ mullite ceramic using waste rice husk ash-derived silica, J. Eur. Ceram. Soc. 42 (5) (2022) 2408–2419, https://doi.org/10.1016/j.jeurceramsoc.2022.01.001.
[14] K. Huang, H. Elsayed, G. Franchin, P. Colombo, Complex SiOC ceramics from 2D structures by 3D printing and origami, Addit. Manuf. 33 (2020), 101144, https://doi.org/10.1016/j.addma.2020.101144.
[15] E. Zanchetta, M. Cattaldo, G. Franchin, M. Schwentenwein, J. Homa, G. Brusatin, P. Colombo, Stereolithography of SiOC ceramic microcomponents, Adv. Mater. 28 (2) (2016) 370–376, https://doi.org/10.1002/adma.201503470.
[16] C. He, X. Liu, C. Ma, X. Li, F. Hou, L. Yan, A. Guo, J. Liu, Digital light processing fabrication of mullite component derived from preceramic precusor using photosensitive hydroxysiloxane as the matrix and alumina nanoparticles as the filler, J. Eur. Ceram. Soc. 41 (11) (2021) 5570–5577, https://doi.org/10.1016/j.jeurceramsoc.2021.04.051.
[17] J. Schmidt, A.A. Altun, M. Schwentenwein, P. Colombo, Complex mullite structures fabricated via digital light processing of a preceramic polysiloxane with active alumina fillers, J. Eur. Ceram. Soc. 39 (4) (2019) 1336–1343, https://doi.org/10.1016/j.jeurceramsoc.2018.11.038.
[18] M. Pelanconi, P. Colombo, A. Ortona, Additive manufacturing of silicon carbide by selective laser sintering of PA12 powders and polymer infiltration and pyrolysis, J. Eur. Ceram. Soc. 41 (10) (2021) 5056–5065, https://doi.org/10.1016/j.jeurceramsoc.2021.04.014.
[19] L. Gorjan, R. Tonello, T. Sebastian, P. Colombo, F. Clemens, Fused deposition modeling of mullite structures from a preceramic polymer and γ-alumina, J. Eur. Ceram. Soc. 39 (7) (2019) 2463–2471, https://doi.org/10.1016/j.jeurceramsoc.2019.02.032.
[20] A. Kulkarni, J. Pearce, Y. Yang, A. Motta, G.D. Sorarù, SiOC (N) cellular structures with dense struts by integrating fused filament fabrication 3D printing with polymer-derived ceramics, Adv. Eng. Mater. 23 (12) (2021), 2100535, https://doi.org/10.1002/adem.202100535.
[21] P. Colombo, J. Schmidt, G. Franchin, A. Zocca, J. Günster, Additive manufacturing techniques for fabricating complex ceramic components from preceramic polymers, Am. Ceram. Soc. Bull. 96 (3) (2017) 16–23.
[22] F. Sarraf, E. Abbatinali, L. Gorjan, T. Sebastian, P. Colombo, S.V. Churakov, F. Clemens, Effect of MgO sintering additive on mullite structures manufactured by fused deposition modeling (FDM) technology, J. Eur. Ceram. Soc. 41 (13) (2021) 6677–6686, https://doi.org/10.1016/j.jeurceramsoc.2021.06.012.
[23] P. Colombo, E. Bernardo, G. Parcianello, Multifunctional advanced ceramics from preceramic polymers and nano-sized active fillers, J. Eur. Ceram. Soc. 33 (3) (2013) 453–469, https://doi.org/10.1016/j.jeurceramsoc.2012.10.006.
[24] S. Walter, D. Suttor, T. Erny, B. Hahn, P. Greil, Injection moulding of polysiloxane/filler mixtures for oxycarbide ceramic composites, J. Eur. Ceram. Soc. 16 (4) (1996) 387–393, https://doi.org/10.1016/0955-2219(95)00120-4.

[25] F. Wolff, B. Ceron Nicolat, T. Fey, P. Greil, H. Münstedt, Extrusion foaming of a preceramic silicone resin with a variety of profiles and morphologies, Adv. Eng. Mater. 14 (12) (2012) 1110–1115, https://doi.org/10.1002/adem.201100351.
[26] L. Fiocco, E. Bernardo, Novel cordierite foams from preceramic polymers and reactive oxide fillers, Mater. Lett. 159 (2015) 98–101, https://doi.org/10.1016/j.matlet.2015.06.100.
[27] D. Hotza, R.K. Nishihora, R.A. Machado, P.M. Geffroy, T. Chartier, S. Bernard, Tape casting of preceramic polymers toward advanced ceramics: A review, Int. J. Ceram. Eng. Sci. 1 (1) (2019) 21–41, https://doi.org/10.1002/ces2.10009.
[28] A. Guo, M. Roso, M. Modesti, J. Liu, P. Colombo, Preceramic polymer-derived SiOC fibers by electrospinning, J. Appl. Polym. Sci. 131 (3) (2014) n/a, https://doi.org/10.1002/app.39836.
[29] Z. Yang, Z. Zhao, J. Yu, Z. Ren, Preparation of silica ceramic cores by the preceramic pyrolysis technology using silicone resin as precursor and binder, Mater. Chem. Phys. 223 (2019) 676–682, https://doi.org/10.1016/j.matchemphys.2018.11.039.
[30] P. Colombo, J.R. Hellmann, Ceramic foams from preceramic polymers, Mater. Res. Innov. 6 (5) (2002) 260–272, https://doi.org/10.1007/s10019-002-0209-z.
[31] E. Ionescu, R. Riedel, Polymer Processing of Ceramics, Wiley, Hoboken, NJ, USA, 2012.
[32] P. Greil, Active-filler-controlled pyrolysis of preceramic polymers, J. Am. Ceram. Soc. 78.4 (1995) 835–848, https://doi.org/10.1111/j.1151-2916.1995.tb08404.x.
[33] P. Greil, Polymer derived engineering ceramics, Adv. Eng. Mater. 2.6 (2000) 339–348, https://doi.org/10.1002/1527-2648(200006)2:6<339::AID-ADEM339>3.0.CO;2-K.
[34] W.W. Yang, K.Y. Yang, M.C. Wang, M.H. Hon, Solvent debinding mechanism for alumina injection molded compacts with water-soluble binders, Ceram. Int. 29 (7) (2003) 745–756, https://doi.org/10.1016/S0272-8842(02)00226-2.
[35] X. Yang, C. Jia, Z. Xie, W. Liu, Q. Liu, Water-soluble binder system based on polymethyl methacrylate and poly-ethylene glycol for injection molding of large-sized ceramic parts, Int. J. Appl. Ceram. Technol. 10 (2) (2013) 339–347, https://doi.org/10.1111/j.1744-7402.2011.02745.x.
[36] V.A. Krauss, A.A.M. Oliveira, A.N. Klein, H.A. AlQureshi, M.C. Fredel, A model for PEG removal from alumina injection moulded parts by solvent debinding, J. Mater. Process. Technol., 182(1-3) (182 (2007) 268–273, https://doi.org/10.1016/j.jmatprotec.2006.08.004.
[37] M.I. Baker, S.P. Walsh, Z. Schwartz, B.D. Boyan, A review of polyvinyl alcohol and its uses in cartilage and orthopedic applications, J. Biomed. Mater. Res. Part B Appl. Biomater. 100 (5) (2012) 1451–1457, https://doi.org/10.1002/jbm.b.32694.
[38] T.F. McNulty, F. Mohammadi, A. Bandyopadhyay, D.J. Shanefield, S.C. Danforth, A. Safari, Development of a binder formulation for fused deposition of ceramics, Rapid Prototyp. J. 4 (4) (1998) 144–150, https://doi.org/10.1108/13552549810239012.
[39] M. Jafari, W. Han, F. Mohammadi, A. Safari, S.C. Danforth, N. Langrana, A novel system for fused deposition of advanced multiple ceramics, Rapid Prototyp. J. 6 (3) (2000) 161–175, https://doi.org/10.1108/13552540010337047.
[40] F. Clemens, J. Schulz, L. Gorjan, A. Liersch, T. Sebastian, F. Sarraf, Debinding and sintering of dense ceramic structures made with fused deposition modeling. International Conference on Additive Manufacturing in Products and Applications, Springer, 2020, pp. 293–303, https://doi.org/10.1007/978-3-030-54334-1_21.
[41] A. Hadian, L. Koch, P. Koberg, F. Sarraf, A. Liersch, T. Sebastian, F. Clemens, Material extrusion based additive manufacturing of large zirconia structures using filaments with ethylene vinyl acetate based binder composition, Addit. Manuf. 47 (2021), 102227, https://doi.org/10.1016/j.addma.2021.102227.
[42] F.J. Clemens, A. Kerber, FDM/FFF an alternative to CIM manufacturing of prototype and small quantities of ceramic part, Ceram. Appl. 8 (2020) 27–31.
[43] N. Venkataraman, S. Rangarajan, M.J. Matthewson, B. Harper, A. Safari, S. C. Danforth, G. Wu, N. Langrana, S. Guceri, A. Yardimci, Feedstock material property–process relationships in fused deposition of ceramics (FDC), Rapid Prototyp. J. 6 (4) (2000) 244–253, https://doi.org/10.1108/13552540010373344.
[44] A. Bellini, L. Shor, S.I. Guceri, New developments in fused deposition modeling of ceramics, Rapid Prototyp. J. 11 (4) (2005) 214–220, https://doi.org/10.1108/13552540510612901.
[45] A. Hadian, C. Zamani, L. Gorjan, F.J. Clemens, Thermoplastic processing and debinding behavior of NbC-M2 high speed steel cemented carbide, J. Mater. Process. Technol. 263 (2019) 91–100, https://doi.org/10.1016/j.jmatprotec.2018.08.006.
[46] T.H. Ku, C.A. Lin, Shear flow properties and melt spinning of thermoplastic polyvinyl alcohol melts, Text. Res. J. 75 (9) (2005) 681–688, https://doi.org/10.1177/0040517505059207.
[47] J. Heiber, F.J. Clemens, T. Graule, D. Hülsenberg, Influence of varying the powder loading content on the homogeneity and properties of extruded PZT-fibers, Key Eng. Mater. 368 (2008) 11–14, https://doi.org/10.4028/www.scientific.net/KEM.368-372.11.
[48] P.S. Thomas, J.P. Guerbois, G.F. Russell, B.J. Briscoe, FTIR study of the thermal degradation of poly (vinyl alcohol), J. Therm. Anal. Calorim. 64 (2) (2001) 501–508, https://doi.org/10.1023/A:1011578514047.
[49] K. McGarry, J. Zilberman, T.R. Hull, W.D. Woolley, Decomposition and combustion of EVA and LDPE alone and when fire retarded with ATH, Polym. Int. 49 (10) (2000) 1193–1198, https://doi.org/10.1002/1097-0126(200010)49:10<1193::AID-PI537>3.0.CO;2-0.
[50] N. Chuaponpat, T. Ueda, A. Ishigami, T. Kurose, H. Ito, Morphology, thermal and mechanical properties of co-continuous porous structure of pla/pva blends by phase separation, Polymers 12 (5) (2020) 1083, https://doi.org/10.3390/polym12051083.
[51] A.M. Henderson, Ethylene-vinyl acetate (EVA) copolymers: a general review, IEEE Electr. Insul. Mag. 9 (1) (1993) 30–38, https://doi.org/10.1109/57.249923.